Parametric investigation of the fluid mechanic performance of an AC dielectric barrier discharge plasma actuator.

Sylvain Grosse‡ and David Angland§

University of Southampton, Boldrewood Campus, Burgess Road, Southampton SO16 7QF UK

E-mail: S.Grosse@soton.ac.uk, D.Angland@soton.ac.uk

Abstract.

The aim of this work is to systematically quantify and rank the effects of nine different design parameters on the fluid mechanic abilities of a Dielectric Barrier Discharge (DBD) plasma actuator supplied with an Alternating Current. The ranking and quantification not only consider the parameters themselves but also their interactions with each other. In order to perform this ranking, a Design of Experiment approach is used. This allows the most significant design parameters for the thrust generation, power consumption and thrust to power consumed ratio (force efficiency) of DBD actuator performance to be determined in a systematic way. The results show that the thrust generation is driven by the voltage, distance between the electrodes, AC frequency, and geometry of the exposed electrode, in that order. A high voltage and high frequency, with a thin dielectric, a narrow inter-electrode gap, and a thin and narrow air-electrode results in an increase in the thrust generation.The thrust to power ratio of a DBD is employed as a proxy for the fluid mechanic efficiency. The analysis of the force efficiency shows that the voltage, frequency, distance between the electrodes, and geometry of the air electrode have significant effects. The higher force efficiency is obtained for a high voltage, low frequency, short inter-electrode gap, thin dielectric of low permittivity with a narrow and thin exposed electrode. Finally, two actuators are investigated to determine the best scaling laws for the power consumption as a function of voltage and frequency. In these experiments, the power consumption was a function of voltage to the power of 2.5 and frequency to the power of 1.5. This systematic study of the parameters and their interactions allows general guidelines to be obtained for the best fluid mechanic performance of a DBD, viz. its thrust generation and force efficiency.

Keywords: dielectric barrier discharge, DBD, flow control, plasma, design of experiment, DOE

Submitted to: *J. Phys. D: Appl. Phys.*

‡ Alternate email: sylvain.grosse@laposte.net, ORCID: 0000-0002-0365-1357
§ ORCID: 0000-0001-5451-2763

1. Introduction

The standard arrangement of a Dielectric Barrier Discharge (DBD) plasma actuator consists of two electrodes separated by a dielectric layer (see Figure 1). One electrode is encapsulated in a dielectric material, and the second is exposed to air. A high-voltage is applied, resulting in the generation of plasma. The charged species drift between the air-exposed electrode and the surface of the dielectric due to electromagnetic forces. Thus, a wall jet is induced by the plasma, as a result of the collisions between the neutral and charged particles. This wall jet can be modeled as a Glauert laminar wall jet [1], that extends a few millimeters over the surface of the actuator [2].

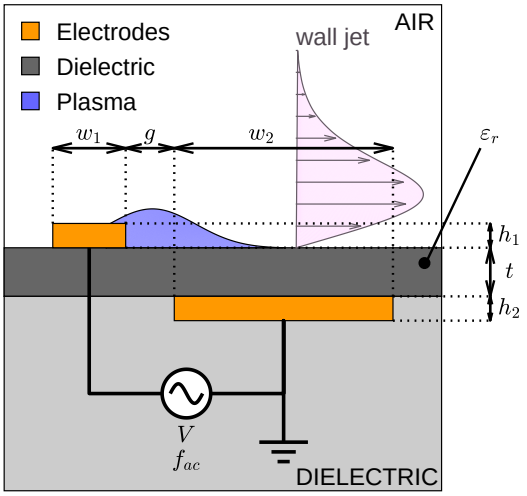

Figure 1: Typical DBD configuration and characteristics.

The flow control abilities of DBDs are now well established for applications such as boundary layer control [3, 4, 5], or flow control over simple geometries [6, 7, 8] at low Reynolds number. Also, their ease of production and installation make them a suitable candidate for flow control applications. However, the induced velocity is relatively low (maximum of 5 to 10 m/s close to the wall), thus limiting the control authority of the DBD.

Kriegseis *et al* [9] presented the power-flow diagram of a DBD actuator for flow control focusing on four stages. The first stage is the overall power supplied by the power source, which is named "input power" by the authors. Part of this power is lost through electrically resistive effects when generating plasma. The second stage is the "actuator power". However, the plasma generated by the actuator has its own efficiency measured by its ability to convert its electrical power into a body force in the fluid. Therefore, the third stage is the "fluid mechanic power", which corresponds to the actual power imparted by the DBD to the fluid. Finally, the actuator can be used for a specific flow control application, which will dictate its placement and the modulation of its electrical input. A key part of this entire process is to obtain an actuator that induces a high momentum into the flow with the lowest power usage (to transform electrical power into fluid mechanic power). This present work focuses on this particular stage where the actuator power is transferred to a momentum injection in the fluid by a DBD. Consequently, it restricts to what Kriegseis *et al* [9] refer to as the "fluid mechanic efficiency". Depending on the specific application, the efficiency of the actuator can be further enhanced, by modulating the signal [7, 10, 11, 12] at specific excitations frequencies for the particular application.

For a DBD supplied with a time varying electric current, several parameters can be adjusted to maximize the induced thrust and minimize the consumed power. The parameters are shown in Figure 1. They are the width and height of the air-exposed (w_1 and h_1) and encapsulated (w_2 and h_2) electrodes, the inter-electrode gap (g), the thickness of the dielectric layer (t), the permittivity of the dielectric material (ε_r), and the voltage (V) and frequency (f_{ac}) of the electric signal. The waveform of the time varying current can also be modified. However, in this study only the most common waveform is considered, viz. a sine wave.

At a fixed voltage, Forte *et al* [13, 14] observed that a thinner dielectric thickness increases the maximum velocity induced by the plasma. They also showed that, for a given consumed power, a lower permittivity of the dielectric increases the maximum induced velocity. Moreover, Thomas *et al* [15] highlighted that, at a constant voltage and frequency, decreasing the dielectric thickness or permittivity increases the thrust. They also described a phenomenon of thrust saturation when the plasma discharge transitions from a uniform glow discharge to a heterogeneous filamentary discharge. The thrust initially scales as voltage to the power of 3.5, but as saturation is approached, the thrust scales as voltage to the power of 2.3. When the saturation is reached, the thrust stagnates at a value that reduces if the frequency or dielectric permittivity increases. However, the authors highlighted that a thick dielectric of high permittivity can practically sustain higher voltages before reaching breakdown, and hence achieve a greater thrust. Forte *et al* [13, 14] proved a small inter-electrode gap (g) of 0 to 5 mm leads to a greater maximum velocity in the induced wall jet. As a first approximation, Murphy *et al* [2] noticed an inverse relationship between the consumed power and dielectric thickness (t). This trend could be explained by the power loss occurring inside the dielectric layer,

due to the polarization of the electric charges. It is proportional to ε_r/t, as indicated by Corke *et al* [10].

The material of the electrodes was not found to influence the performance of the DBD, as highlighted by Hoskinson *et al* [16]. A thinner exposed electrode was seen to give a higher thrust generation and a higher force efficiency (thrust over power ratio). This phenomenon was seen especially for wire type exposed electrode by Hoskinson *et al* [16], Enloe *et al* [17] and Debien *et al* [18]. It can hence be expected that a thin and narrow rectangular exposed electrode would provide a higher thrust and force efficiency. Abe *et al* [19] assessed a mesh type exposed electrode that created a stronger electric field than a standard plain electrode. It produced more thrust than a simple rectangular electrode at various ambient pressures. However, a wire mesh was not evaluated against a mesh electrode.

Although the thickness of the encapsulated electrode (h_2) was not particularly studied, its width (w_2) plays an important role in the momentum induction by the plasma. A narrow encapsulated electrode can constrain the plasma, hence limiting its extent over the dielectric surface, as described by Forte *et al* [13], Thomas *et al* [15] and Enloe *et al* [17]. If the encapsulated electrode is wide enough not to constrain the plasma extent, increasing its width (w_2) does not further improve the thrust generated by the actuator [13, 15].

Increasing the voltage or frequency of the electric signal increases both the thrust generation and the power consumption. Enloe *et al* [17], Debien *et al* [18] and Abe *et al* [19] concluded that an almost linear relationship existed between the induced thrust and the consumed power. It is typically agreed that the maximum induced velocity [10, 15, 20] and the power consumption [10, 15, 17, 21, 22] are proportional to the voltage to the power 7/2. However, some discrepancies exist in the reported power laws. For instance, the power consumption has been observed to be proportional to the square of the voltage [13, 23, 24]. Experiments reveal the consumed power depends on the frequency to a power ranging between 1 [19] and 1.5 [21]. A linear relationship between the power and the frequency can be expected, since the consumed power over one AC period is defined by the energy consumed over this period multiplied by the frequency of the AC signal [21]. Any other dependency of the power on the frequency is caused by the discharge, and affects the consumed energy. Kriegseis *et al* [21] proposed a scaling parameter Θ_A based on the commonly reported scaling laws,

$$\Theta_\mathrm{A} = \frac{\Pi_\mathrm{A}/L}{V^{3.5} f_\mathrm{ac}^{1.5}} \quad , \tag{1}$$

where Π_A is the power consumption in watts, L the electrode span, V the voltage and f_ac the frequency. However, this parameter is not non-dimensional, and has a dependency on the design of the actuator. The influence of the waveform was analyzed by different authors [10, 25, 22, 26]. It was observed a sine or triangular wave with a longer negative going half cycle and shallow positive going half cycle enhances the momentum transfer to the flow. The rectangular wave was found inefficient compared to the other two waveforms [10]. However, with a very high frequency (tens of kilovolts) and a low duty cycle, the rectangular wave can be tuned into nanosecond pulses. The momentum injection by the nanosecond-pulsed DBDs (NS-DBDs) and AC driven DBDs are different [27, 28]. NS-DBDs create a fast discharge, that leads to a high temperature and pressure jump, generating a flow through thermal effects. On the other hand, AC driven DBDs induce momentum in the flow through electrohydrodynamic forcing.

Some considerable work has already been performed in order to determine the influence of numerous design parameters on the ability of the DBD to produce thrust at a given electrical power consumption. However, it has not been performed systematically, ranking and quantifying the effects of the different design parameters. It is also uncertain how these different factors interact with each other, and whether these potential interactions impact the fluid mechanic performance of the actuator, here defined as its thrust generation and force efficiency. This current work addresses these points.

In order to rank and quantify the parameters and their interactions, a Design of Experiment (DOE) [29] approach is used in this work. The method enables the most significant geometric and electrical parameters to be determined, and quantify how they affect the fluid mechanic performance of DBDs. It also allows the interactions between the different parameters to be examined. The method can also be used to derive simple linear regression models to predict the flow control performance of a DBD with a given design. The experimental rig used in the experiments in described in Section 2. The ranking of parameters and their interaction for thrust, power consumption and force efficiency (thrust/power consumption) are presented in Sections 3, 4 and 5 respectively. Finally, in Section 6, the observed scaling laws are discussed.

2. Experimental method

2.1. Electrical measurements

The high voltage source comprises of two pieces of equipment. A low voltage signal is delivered by a BK Precision 4010A function generator, and amplified by a Trek 20/20C-HS high-voltage amplifier. The

frequency of the voltage is derived from the TTL signal emitted by the function generator. The voltage and current are measured by the amplifier in-built voltmeter and ammeter with accuracies of 20 V for the output voltage and 0.2 mA for the output current, with full scales of 20 kV of amplitude and 20 $\mathrm{mA_{rms}}$. These monitors provide the time averaged quantities. The consumed power Π_A is obtained by the integration of the product of the voltage V and current I over n periods τ_ac $(= 1/f_\mathrm{ac})$ of the AC signal,

$$\Pi_\mathrm{A} = \frac{1}{n\tau_\mathrm{ac}} \left(\int_0^{n\tau_\mathrm{ac}} V I \, \mathrm{d}t \right) \quad . \tag{2}$$

In the present work, n is 2500 for the frequency of 0.5 kHz and 10000 for the frequency of 2.0 kHz. The acquisition is performed by a dSpace DS1104 board, with 5 s recordings sampled at 40 kHz (2.0×10^5 points per sample). The standard error for the full scale with 2.0×10^5 observations is 0.009 W. The two-tailed Student's t-value for 2.0×10^5 points with a confidence level of 95% is 1.96, giving a confidence interval of ± 0.02 W.

It is also important to note that the electrically capacitive behavior of the DBD is responsible for a phase shift between the electrical current and voltage (on average 85 degrees in the present study). If the Trek 20/20C-HS power supply exceeded its distortion limit, it would trip. To avoid this, the voltage and frequency ranges discussed in Section 2.3 were selected in order to achieve the maximum capacitance within the capabilities of the Trek 20/20C-HS amplifier. Supplementary tests showed that the amplifier would trip around 17 to 18 $\mathrm{kV_{pp}}$ for several of the DBDs used in the study.

2.2. Force measurements

The momentum transferred to the free-stream is measured through the thrust produced by the DBD actuators. The force measurement is realized by a dedicated test rig, that amplifies the thrust via a lever (see Figure 2). The amplification ratio by the lever is 9.2. In order to lower the friction in the linkage between the lever and its support, a straight blade was utilized. As a result, the lever lies on a sharp blade, where it is balanced by three calibration masses as shown in Figure 2. The force is recorded by a NovaTech F329 deci-Newton load cell with an accuracy of 10 μN, on a full scale of 100 mN. Consequently, the test rig provides measurements up to 10.9 mN. The entire test rig is enclosed in a perspex box, so that it is isolated from free-stream disturbances. The box and its dimensions are shown in Figure 3. The acquisition is performed by a dSpace DS1104 board, with 5 s samples obtained at a frequency of 25 kHz (1.25×10^5 points per sample). The standard deviation measured on the signal from the test rig at full scale is 105 μN, leading to a standard error of $105/\sqrt{1.25 \times 10^5} = 0.3$ μN. For a confidence level of 95%, the two-tailed Student's t-value for each sample is 1.96. Hence, the confidence interval of the rig is ± 0.6 μN for each data point acquired with the experimental rig.

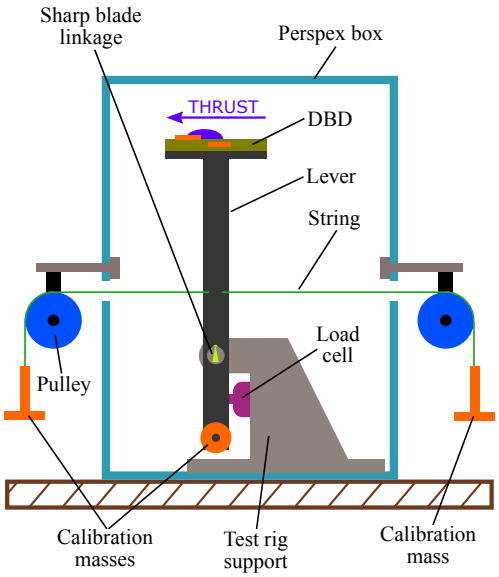

Figure 2: Schematic of test rig for micro-thrust measurement. N.B. not to scale.

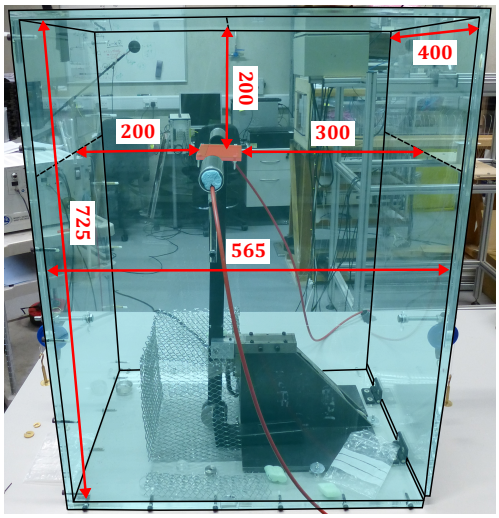

Figure 3: Picture of test rig for micro-thrust measurements in its perspex box. Dimensions in millimetres.

2.3. Design of experiments and DBD actuators

All the DBDs utilized in this study were produced using standard printed circuit board manufacturing techniques. This is done to minimize the impact of

inaccuracies and variability in the production process on the final results. However, it also means several of the nine parameters (see Figure 1) are limited to particular sets of values due to manufacturing constraints. This led to the use of a standard 2-level fractional factorial Design of Experiment (DOE) approach. In this approach, each of the design parameters can take two values.

A full factorial design evaluates all the possible combinations of parameter values, and would require to $2^9 = 512$ independent tests. 512 tests would not be feasible in a reasonable time frame, especially if they are to be repeated to gain in accuracy. In order to reduce the number of experimental data points, a 1/16 fraction was chosen, resulting in $2^{9-4} = 32$ separate runs. Each run corresponds to a particular set of low and high values of the nine factors, and all the runs are unique. The test matrix is a standard Plackett-Burman design with 32 runs, for 9 design parameters with a 1/16 fraction. The test matrix was also randomized before commencing the experimental campaign.

Due to this reduction of the number of experimental tests, all the combinations of levels of the variables are not met. Hence, the interactions between the design parameters can only be analyzed between up to two interacting parameters. Moreover, aliases between some interactions exist in the results, meaning the analysis cannot differentiate whether one observed effect is caused by one interaction or its alias(es). The aliases are systematically described in the discussion of the results. An interaction occurs when the influence of a design variable on the output parameter is altered by another design variable.

The 32 runs were all performed three times, in order to reduce the uncertainty of the results. Consequently, the final test matrix includes $32 \times 3 = 96$ data points in total. The design was realized and analyzed using Minitab 18.

The low and high values of all the parameters represented in Figure 1 are given in Table 1. The dielectric material is either standard FR4 epoxy laminate ($\varepsilon_r = 4.42$) or glass reinforced PTFE laminate ($\varepsilon_r = 2.33$). The electrodes are all made of copper, and all have a span L of 100 mm. The variables in Table 1 have different ranges between the maximum and minimum values tested. These ranges were selected based on the existing literature, presented in section 1, and based on manufacturing limitations of the PCBs used as the actuators. Therefore, the following analysis compares the effects of the nine parameters and their interactions within the selected ranges in the design of experiment. It is important to note that this analysis cannot necessarily be extended outside of these ranges with any certainty. The effects and their ranking therefore depend on the chosen ranges to some extent. All the actuators have the same longitudinal and lateral dimensions of 70 mm × 110 mm (see Figure 4). The encapsulated electrode front edge is located 54.5 mm from the rear edge of the actuator for all DBDs. In the case where the electrodes have two different copper thickness, two printed circuit boards are bonded together with an epoxy glue 0.5 mm from the encapsulated electrode (i.e. 55 mm from the rear edge of the actuator, see Figure 4). Three output parameters are analyzed:

- The thrust generation by the actuator per unit of electrode span T_A (mN/m).
- The consumed power by the actuator per unit of electrode span P_A (W/m).
- The force efficiency of the actuator $\eta_\mathrm{A} = T_\mathrm{A}/P_\mathrm{A}$ (μN/W).

Parameter	**Symbol (units)**	**Low and high values**
Exposed electrode width	w_1 (mm)	0.5 5
Encapsulated electrode width	w_2 (mm)	10 50
Inter-electrode gap	g (mm)	1 5
Exposed electrode height	h_1 (μm)	35 70
Encapsulated electrode height	h_2 (μm)	35 70
Dielectric layer thickness	t (mm)	0.8 3.2
Permittivity of the dielectric	ε_r	2.33 4.42
Applied voltage	V ($\mathrm{kV_{pp}}$)	10 16
Signal frequency	f_ac (kHz)	0.5 2

Table 1: Studied parameters in the Design of Experiments.

The DOE analysis draws linear regression models based on the different design parameters and their interactions. Mathematically, if Y is the output parameter and X is the array of the input variables, the linear regression model is represented by the lower triangular matrix A defined by,

$$X = \begin{bmatrix} 1 & w_1 & w_2 & g & h_1 & h_2 & t & \varepsilon_r & V & f_\mathrm{ac} \end{bmatrix}, \quad (3)$$

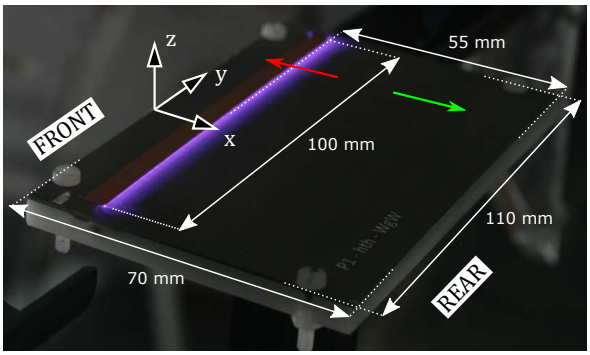

x	Longitudinal direction.
	Streamwise direction.
	Counter-streamwise direction.
y	Spanwise directions.
z	Wall normal direction.

Figure 4: DBD actuator and its characteristic dimensions.

$$Y = X \cdot M \cdot X^{\mathrm{T}} \quad . \tag{4}$$

In Equation 3, the first term needs to be a constant (1 for simplicity), so that the model can adjust the zero intercept, and determine the coefficients for the single factors, making its length equal to the number of input parameters plus one. The derivation of the model requires the errors between the measurements and predictions to be normally distributed. Therefore, it is common to transform the output variable through an increasing monotonic function (power law or natural logarithm typically) so that this assumption is obeyed. The DOE model is calculated for the transformed response in this case. The employed transformations are detailed in the discussion of the results. The main disadvantage of the models is their limitation to simple mathematical functions. They also average the behavior of the DBDs across all the runs, even if the different actuators can generate distinct types of plasma discharges that could obey different mathematical scaling laws. This point is discussed in the analysis of the models.

In the construction of the model, all the parameters and their interactions are not included. The analysis of a DOE relies on the observed changes in the mean value of the output parameter due to a change in value of a design variable. For instance in the present study, the effect of w_1 on the thrust T_{A} is the difference in the average of the thrust over all the tests for which $w_1 = 5$ mm and the average of the thrust over all the tests for which $w_1 = 0.5$ mm. From the 96 tests, half are assigned to either one of the two levels of each design variable. Mathematically, the effect E of w_1, can be expressed as,

$$E = \frac{\sum \left(T_{\mathrm{A}}\left(w_1 = 5\ \mathrm{mm}\right)\right)}{48} - \frac{\sum \left(T_{\mathrm{A}}\left(w_1 = 0.5\ \mathrm{mm}\right)\right)}{48} \quad .(5)$$

The statistically significant effects are selected by comparing their distribution to the normal distribution. The normally distributed effects are attributed to random errors and the residuals that are not included in the model. In order to confirm the insignificance of the neglected effects, they are transformed into standardized effects. A standardized effect is Student's t-value of the risk that the observed effect is due to random error. For 96 observations, a standardized effect SE is defined as,

$$SE = \frac{|E|}{\sqrt{MS_{\mathrm{res}}\left(1/48 + 1/48\right)}} \quad , \tag{6}$$

where $|E|$ is the absolute value of the effect and MS_{res} the mean square of the residual effects chosen previously. A critical t-value can be calculated based on the desired confidence level and number of data points. In the present study, a confidence level of 95% was selected with 96 tests, leading to a two tailed t-value of 1.98. A statistically significant effect has a standardized effect greater than this critical t-value.

3. Significant effects on the thrust generation

The analysis of the thrust generation is performed on the square root of the thrust, in order to satisfy the normal distribution of the residuals discussed in the previous section. The analysis identified nineteen statistically significant effects. These nineteen model terms are responsible for 97.4% of the total variance captured in the data. 91% of the variance of the results is due to only nine parameters and interactions. The standardized effects are presented in descending

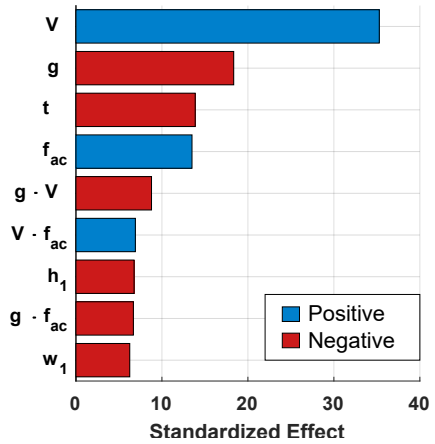

Figure 5: Pareto chart of the standardized effects on the thrust generation colored by sign of the effects.

order in the Pareto chart in Figure 5 for these nine most significant effects. All the displayed standardized effects are greater than a critical t-value of 1.98. The bars are colored by sign of the original effects (i.e. a positive increase in a parameter increases the thrust and vice versa). For each original effect, the means are obtained over 48 data sets for the effects of the single factors, and 24 for the interactions, each having a confidence interval of ± 6 μN/m of electrode span. The Student's t-value for 48 and 24 observations with a confidence level of 95% are 2.01 and 2.06 respectively. As a result, the confidence intervals of the mean of the thrust described in the next paragraphs are ± 1.8 μN/m for the single factors and ± 2.5 μN/m for the interactions. The statistically significant effects on thrust are discussed below in order of significance.

3.1. Voltage

The voltage (V) plays a major positive effect of 0.268 mN/m/kV$_{\mathrm{pp}}$ on the thrust generation. This result is not surprising, since increasing the voltage increases the electric field across the electrodes, and hence the ion drift velocity. As it can be found in the work of Kriegseis et al. [30], the ion drift velocity v_{d} can be expressed as the electric field E multiplied by an ion mobility coefficient κ:

$$v_{\mathrm{d}} = \kappa E \ . \tag{7}$$

It can be approximated that the electric field is the ratio of the potential difference between the electrodes over the distance separating them [30]. By using the Pythagorean theorem to the present case, the electrode are set apart by the distance $\sqrt{g^2 + t^2}$. Hence, Equation 7 results in:

$$v_{\mathrm{d}} = \kappa \frac{V}{\sqrt{g^2 + t^2}} \ ; \ . \tag{8}$$

However, Equation 8 is only a rough approximation as it does not take into account the difference in permittivity between the gaseous species and the dielectric. An increase in the voltage also increases the number of charged particles in the plasma.

3.2. Separation of the electrodes

In Equation 8, the inter-electrode gap (g) and dielectric thickness (t) are the next significant parameters, with respective losses of 0.210 and 0.263 mN/m/mm. The loss of thrust with a thicker dielectric agrees with the literature [13, 14, 15]. Both effects have a comparable amplitude, but there is a measurable difference between the effect of electrode gap and the effect of dielectric thickness. One explanation for this could be the higher permittivity of the dielectric compared to air, leading to a larger drop in the electric field if the dielectric layer thickness increases, compared to the case where the inter-electrode gap increases.

3.3. Frequency

The fourth significant factor is the AC frequency (f_{ac}) with a positive effect of 0.407 mN/m/kHz on the thrust generation. Qualitatively, the increase agrees with previous published work [13, 15, 19]. It indicates that the momentum transfer is increased by a higher AC frequency, due to a greater collision frequency between the charged particles and the neutral gas species.

3.4. Interactions of the gap with the voltage and frequency

The interactions between either the gap or the dielectric thickness and either the voltage or frequency, i.e. $g \times V$, $g \times f_{\mathrm{ac}}$, $t \times V$ and $t \times f_{\mathrm{ac}}$ proved that the improvement with a small electrode separation is greater when the voltage and frequency are at their largest values. This was most significant in the case of the interaction between the inter-electrode gap and either one of the electrical parameters ($g \times V$ and $g \times f_{\mathrm{ac}}$). Indeed, these two interactions were found to be significant in the Pareto chart in Figure 5 (ranked 5^{th} and 8^{th} respectively). For a short gap of 1 mm, the gain in thrust reached 0.45 mN/m/kV$_{\mathrm{pp}}$ compared to a lower increase of 0.16 mN/m/kV$_{\mathrm{pp}}$ for a 5 mm gap. Similarly, the thrust has a gain of 0.79 mN/m/kHz for a 1 mm gap compared to only 0.15 mN/m/kHz for a 5 mm gap. The increased significance of the interactions with the inter-electrode gap compared to the dielectric thickness are assumed to come from the lower permittivity of the plasma/air in comparison to the dielectric. According to Gauss's law, the divergence of the electric field is inversely proportional to the permittivity, resulting in a smaller increase in the electric field with a higher permittivity. These results also agree with the observations of Thomas *et al* [15]. In their study, at a constant voltage and frequency, the thrust was found to decrease with increased dielectric thickness.

3.5. Interaction between the voltage and frequency

In Figure 5, the sixth most significant effect on the thrust generation is the interaction between the voltage and frequency ($V \times f_{\mathrm{ac}}$). On average, the thrust increased by 0.16 mN/m/kHz at 10 kV$_{\mathrm{pp}}$, but gained 1.21 mN/m/kHz at 16 kV$_{\mathrm{pp}}$. The more numerous charged particles produced by the high voltage transfer more momentum to the neutral gas, due to the greater collision frequency and velocity of the charged particles at high AC frequency.

3.6. Geometry of the exposed electrode

The geometry of the exposed electrode was also found to be influential while the encapsulated electrode did not particularly affect the thrust generation. The height (h_1) and width (w_1) of the exposed electrode (ranked seventh and ninth in the Pareto chart Figure 5) have negative effects, indicating a thin and narrow air electrode generates more thrust. On average, the narrow electrode was observed to generate 0.29 mN/m more thrust than a wide air electrode. A thin exposed electrode has a similar gain of 0.31 mN/m on average compared to a thick electrode. This agrees with the work of different authors [16, 17, 18]. The lower permittivity of the dielectric was also found to generate a slightly higher thrust (around 0.24 mN/m greater than with the higher permittivity).

3.7. Additional loss of momentum transfer

In addition, a loss of momentum was observed during the experiments. At high voltage and frequency, a narrow exposed electrode was observed to generate plasma on both edges of the electrode, due to the increased electric field. This phenomenon occurred particularly for a thin dielectric and a short inter-electrode gap. This behavior is shown in Figure 6 with two PTFE actuators having the following common parameters: $h_1 = h_2 = 35$ μm, $g = 1$ mm, $t = 0.8$ mm, $\varepsilon_r = 2.33$, $V = 16$ $\mathrm{kV_{pp}}$ and $f_{\mathrm{ac}} = 2$ kHz, but with either wide (top picture, DBD-1, $w_1 = 5$ mm and $w_2 = 50$ mm) or narrow (bottom picture, DBD-2, $w_1 = 0.5$ mm and $w_2 = 10$ mm) electrodes. Additional total pressure measurements were performed that provided additional evidence for the existence of a counter streamwise jet at the front edge of the exposed electrode. The interaction between the width of the exposed electrode and the dielectric thickness ($w_1 \times t$) was found to agree with this observation. However, it is aliased with the interaction $g \times V$ discussed previously. Besides, the interactions between the width of the air electrode and the voltage, frequency or gap were found to be null. Consequently, the interaction $w_1 \times t$ is inconclusive.

The study of the thrust generation reveals several interactions between the design parameters that have significant effects and cannot be ignored. In order to better judge the suitability of a particular design of DBD, it is also important to judge its power consumption, not just the thrust.

4. Significant effects on the power consumption

The analysis of the power is performed on the natural logarithm of the power consumption, so that the residuals of the model are normally distributed as discussed previously. Eighteen statistically significant factors and interactions were identified. The model terms contribute to 99.9% of the variance of the results. Of the variance of the model, 99.4% is due to only five effects. The standardized effects of these five parameters and interactions are presented in Figure 7 in descending order. The colours indicate whether these effects are positive (higher power consumption at high values of the parameter) or negative (lower power consumption at high values of the parameter). All the standardized effects on the figure are greater than the critical t-value of 1.98. Similar to the analysis of the thrust, the mean of the power is obtained over 48 measurements for the single parameters and 24 for the interactions. The single measurements have a confidence interval of ± 0.2 W/m of electrode span. The t-values for the two sample sizes with a 95% confidence level are respectively 2.01 for 48 observations and 2.06 for 24 observations. Thus, the confidence intervals for the means of the power discussed in the following paragraphs are ± 0.03 W/m for the single factor and ± 0.04 W/m for the interactions.

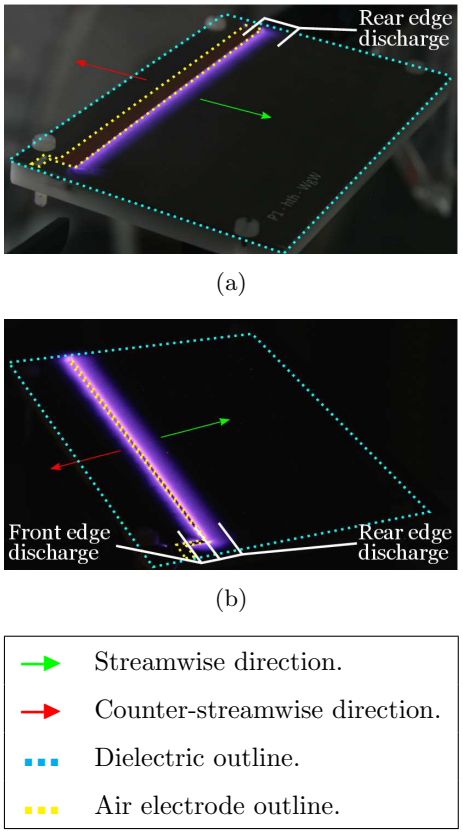

Figure 6: Long exposure pictures of two similar DBDs, (a) DBD-1, $w_1 = 5.0$ mm (wide exposed electrode), (b) DBD-2, $w_1 = 0.5$ mm (narrow exposed electrode).

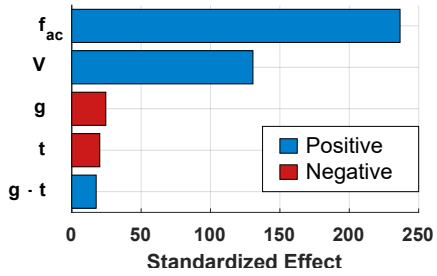

Figure 7: Pareto chart of the standardized effects on the power consumption colored by sign of the effect.

4.1. Electric parameters

The first two important parameters in the Pareto chart Figure 7 are the frequency (f_{ac}) and voltage (V). Both have positive effects on the power consumption with gains of 3.13 W/m/kV$_{pp}$ and 25.3 W/m/kHz. Since the electrical variables were also found to strongly impact the thrust generation, only the analysis of the thrust to power ratio (presented next) can indicate whether each of these factors play a more significant role in the generated thrust or consumed power. Even if the magnitudes of the change in the power consumption cannot be compared, the increase in the power with the electrical variables is consistent with other works [17, 19, 21]. It is also demonstrated that the interaction between the voltage and frequency was found to be the seventh most significant parameter. The increase in power consumption increases from 15.6 W/m/kHz at 10 kV$_{pp}$ to 41.6 W/m/kHz at 16 kV$_{pp}$. This interaction agrees qualitatively with relationships proposed by Kriegseis *et al* [21], who observed that the power depends on the product of the voltage to the power of 3.5, and frequency to the power of 1.5

4.2. Separation of the electrodes

As previously observed in the thrust generation, the inter-electrode gap (g) and dielectric thickness (t) have similar effects. Both parameters have a negative impact on the power consumption, with losses of 0.850 W/m/mm of gap and 1.17 W/m/mm of dielectric thickness. Since an increase in the separation of the electrodes was previously identified as causing a reduction in the thrust generation by weakening the plasma, it is unsurprising that the power consumption decreases if the electrodes are further apart. The greater loss rate of the dielectric thickness compared to the inter-electrode gap concur with the observations realized for the thrust generation. It suggests that the loss of power is linked to the weakening of the discharge that leads to a reduction in thrust generation.

4.3. Interaction between the gap and dielectric thickness

The fifth effect in Figure 7 is the interaction between the gap and dielectric thickness ($g \times t$). The interaction shows that the consumed power, for a large inter-electrode gap, does not vary much with the thickness of the dielectric, but for a short gap, the power increases by 8.6 W/m when the dielectric is thinner. This interaction is a result of the stronger plasma discharge with a shorter separation of the electrodes, leading to a greater power consumption due to the enhanced exchange of charged particles in the plasma.

The power consumption cannot be considered alone for the optimization of the DBD actuators. Several of the significant parameters that impact the power were also observed to improve the thrust generation previously. Consequently, the force over power ratio (or force efficiency) needs to be analyzed to judge the relative importance of the parameters on the thrust and power.

5. Significant effects on the force efficiency

The analysis of the force efficiency is performed on the square root of the efficiency, in order to satisfy the normal distribution of the residuals. The analysis of the force efficiency showed fifteen statistically significant factors and interactions. These model terms are responsible for 91.7% of the variance of the results. However, 90.9% of the variance due to the model can be assigned to nine parameters and interactions. The significant effects are presented in the Pareto chart displayed in Figure 8 in descending order. The colors show the sign of the effects, with a blue color for an increase in force efficiency with an increase in that particular parameter, and red color for a reduction in efficiency with an increase in that parameter. The maximum thrust measured during the test campaign is 0.577 mN $\pm$ 0.6 μN, and the minimum consumed power is 0.29 W $\pm$ 0.02 W. It is important to note that these two values were recorded for two different data points. With the standard propagation of error, the standard error of the force efficiency is 2.5% of the values with an upper bound of 4.34 μN/W. As with the thrust and power, the means of the force efficiency are obtained over 48 observations for the single parameters, and 24 observations for the interactions, with respective t-values of 2.01 and 2.06 at 95% confidence. Consequently, the means discussed in the following paragraphs are given with confidence intervals of 0.22‰ for the single factors and 0.31‰ for the interactions.

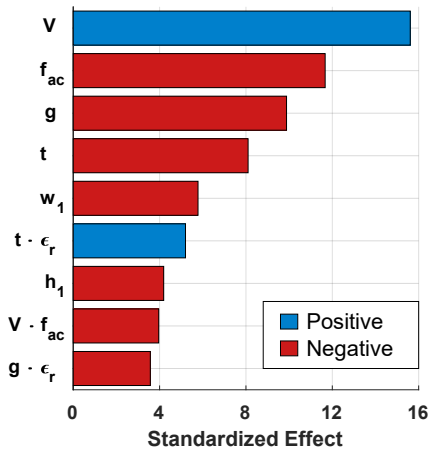

Figure 8: Pareto chart of the standardized effects on the force efficiency colored by sign of the effects.

5.1. Electric parameters

Similar to the thrust generation and power consumption, the electrical parameters and separation of the electrodes form the first four significant effects in the Pareto chart in Figure 8. However, the effects of the voltage (V) and frequency (f_{ac}) have opposite signs with a gain of 7.68 μN/W/kV$_{\text{pp}}$ for voltage and a loss of 23.0 μN/W/kHz for frequency. These two parameters were observed previously to both increase the thrust and power. Hence, the positive effect of the voltage demonstrates that this factor mostly influences the thrust generation. On the contrary, the negative effect of frequency proves it mostly impacts the power consumption. Qualitatively, this effect agrees with the experiments of Thomas *et al* [15], who measured a higher increase in the power consumption compared to the increase in the thrust generation due to an increase in frequency.

5.2. Separation of the electrodes

The next most significant effect in Figure 8 is the separation of the electrodes. As for the thrust and power, the effects of the inter-electrode gap (g) and dielectric thickness (t) are comparable, with losses of 7.33 μN/W/mm of inter-electrode gap and 9.96 μN/W/mm of dielectric thickness. Because the two parameters were found to reduce both the thrust and power, the overall drop in the efficiency demonstrates that a larger separation of the electrodes results in a greater drop in thrust generation. The higher loss rate captured for the dielectric thickness suggests the electric field is further reduced by the dielectric of significant permittivity compared to the air.

5.3. Geometry of the exposed electrode

The fifth and seventh effects in Figure 8 are the width (w_1) and height (h_1) of the air electrode. The effects of the width and thickness are negative, with respective losses of 3.80 μN/W/mm and 0.354 μN/W/μm. Hence, a narrow and thin air electrode improves the force efficiency of the actuator. This trend is in agreement with other observations [16, 18], and demonstrates the higher gain in momentum induced by the plasma discharge caused by a thin and narrow electrode over its consumption of electric power.

5.4. Interactions between the separation of the electrodes and permittivity of the dielectric

The interactions between the thickness and permittivity of the dielectric ($t \times \varepsilon_r$) and between the inter-electrode gap and dielectric permittivity ($g \times \varepsilon_r$) are ranked sixth and ninth in Figure 8 respectively. The interactions are not significant enough to modify the trend previously described (i.e. a shorter distance between the electrodes is overall more efficient). However, the effects are of opposite signs. At either short gap or thick dielectric, the permittivity was not determined to impact the efficiency. On the other hand, for a long gap and thin dielectric, a low permittivity results in respective increases of 23 and 25 μN/W. Because the permittivity was not found to significantly affect the thrust generation or the power consumption, the phenomenon behind this dependency is unsure. Nevertheless, these effects do not change the conclusions previously presented concerning the inter electrode gap and the dielectric thickness. However, it should be noted that the DOE performed in this study predicts a small increase in the force efficiency when reducing the permittivity.

5.5. Interaction between the voltage and frequency

The last significant effect was the interaction between the voltage and frequency ($V \times f_{\text{ac}}$). This interaction was already reported to have a positive effect on the thrust generation. It was also observed to have a less significant positive effect on the power consumption. However, the interaction is negative for the force efficiency. As it was discussed previously, the frequency has a higher effect on the power than it has on the thrust. Conversely, the voltage has a higher effect on the thrust. At 10 kV$_{\text{pp}}$, decreasing the frequency from 2.0 to 0.5 kHz improved the efficiency by 22 μN/W, while the same decrease in frequency resulted in a gain of 61 μN/W at 16 kV$_{\text{pp}}$. Therefore, both increasing the voltage and decreasing the frequency reinforces the individual effects of both of the electrical parameters, and allows a DBD to reach a greater force efficiency.

Several other effects were found to impact the force efficiency, but are only responsible for a small contribution of the variability of the results.

The DOE analysis enables the different design parameters to be ranked in order to determine their significance for the improvement of the flow-control performance of a DBD. The analysis also allows several models to be derived to predict the thrust, power and efficiency of a particular design. Nevertheless, the models rely on linear regression and have a limited ability to capture non-linearity through the interactions and transformations of the responses. In order to verify the scaling of the thrust generation and power consumption with voltage and frequency, two actuators were tested for different voltages and frequencies.

6. Observed scaling laws.

6.1. Description of the two actuators.

The scaling laws of the thrust and power as a function of voltage and frequency were assessed for the two actuators shown in Figure 6. The first design (referred to as DBD-1) was employed in the DOE study at 2.0 kHz and 16 kV_{pp}. It has a wide and thin exposed electrode (5 mm $\times$ 35 μm) and an encapsulated electrode (50 mm $\times$ 35 μm), separated by a short gap (1 mm), and flush-mounted on a a thin PTFE layer (0.8 mm, permittivity 2.33). The second actuator (DBD-2) has a similar geometry, but with narrow exposed and encapsulated electrodes (0.5 mm and 10 mm). It was not included in the original DOE study. Both actuators were experimentally tested every 0.5 kHz between 0.5 and 2.0 kHz, and every 1 kV between 10 and 16 kV_{pp}.

6.2. Scaling of the thrust generation.

The thrust generated by the two actuators were not found to share similar behaviours. For DBD-1, the best power scaling is dependent on the frequency to the power of 0.8 and the voltage to the power of 5.5. This scaling has an adjusted coefficient of determination of 99.6%. On the other hand, the thrust produced by DBD-2 was observed to scale as the frequency to the power of 0.4 and voltage to the power of 2.1, with an adjusted R^2 coefficient of 96.7%. As it can be seen in Figure 6, DBDs 1 and 2 create very different discharges. The plasma ignites on both edges of the exposed electrode of DBD-2, while it only occurs on the rear edge of the electrode for DBD-1. The long exposure pictures of Figure 6 are not able to capture the details in the discharges such as streamers. Consequently, the homogeneity of the discharges cannot be compared, and the differences in the scaling laws are partly due to the different discharge types. As described by Thomas *et al* [15], the thrust is a power law of the voltage, but the power law depends on the closeness to the saturation of the actuator. For instance, the authors observed that the thrust initially depends on voltage to the power of 3.5 but then scales as voltage to the power of 2.3 as the saturation thrust is approached. In the present study, a clear transition of the scaling thrust scaling law with voltage was not unveiled. It is unlikely a common scaling law of thrust with voltage could be determined for all the DBDs employed in the present work because of the different types of discharges that were observed (see Figure 9). These different discharge types exhibit different behaviors, especially when considering the possibility of plasma discharge happening on both edges on some of these DBDs.

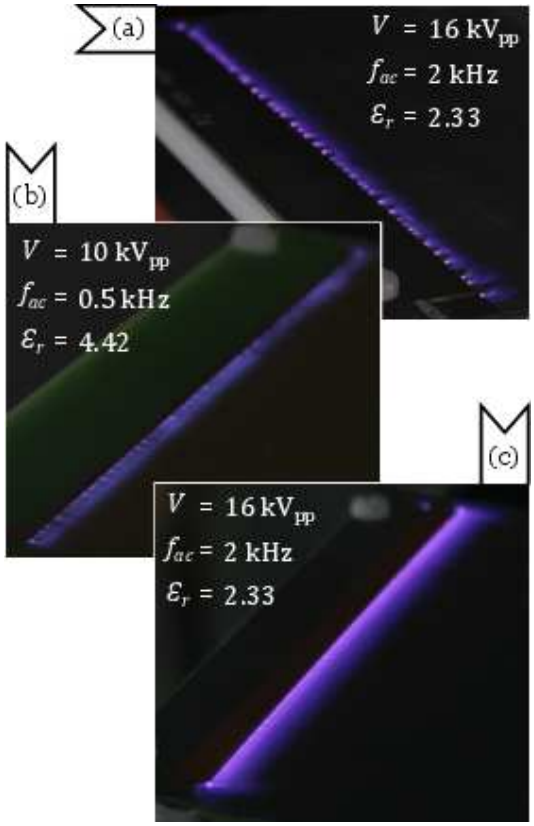

Figure 9: Long exposure pictures of the observed plasma discharges, with (a) filamentary discharge, (b) mixture of filamentary and glow discharge, and (c) glow discharge.

6.3. Scaling of the power consumption.

The scaling of the power can be compared to the work of other authors. In the present study, the power consumption was determined to scale with the frequency to the power of 1.5 and voltage to the power

of 2.5. For this scaling law, the adjusted coefficients of determination are 99.8% for the two actuators. The power consumption of DBD-1 (P_1) and DBD-2 (P_2) in W/m were found to follow the following scaling laws,

$$\begin{bmatrix} P_1 \\ P_2 \end{bmatrix} = \begin{bmatrix} 0.03432 \\ 0.03383 \end{bmatrix} \times f_{\text{ac}}^{1.5} \times V^{2.5} + \begin{bmatrix} 1.339 \\ 2.469 \end{bmatrix}, \quad (9)$$

where f_{ac} is in units of kHz and V is in units of kV_{pp}. The main differences between the two scaling laws is the zero intercept that almost doubles between DBD-1 and DBD-2. The power scaling with the frequency agrees with the conclusion of Kriegseis *et al* [21] with the consumed power scaling as the frequency to the power of 1.5. On the other hand, the power scaling with the voltage is in agreement with the work of other authors [13, 24] with the consumed power depending on the voltage to a power of n, where $2 \leq n \leq 3$.

As was shown in the DOE analysis in Section 4.1 , the consumed power decreases with an increase of voltage or frequency. The main differences between the two actuators are the widths of the air and encapsulated electrodes. The two scaling laws mainly differ by the zero intercept, with an increase of 1.13 W/m of the zero intercept with a decrease of the widths of both electrodes. When considering the ranges employed in the present study for the voltage and frequency, this increase represents between 1 and 20% of the power consumed by DBD-1 and DBD-2. Consequently, the effects of the voltage and frequency dominate the power consumption, but a narrower electrode can lead to an increase in power consumption. The dual plasma discharge shown in Figure 6 certainly contributes to this increased power consumption.

7. Guidance for DBD design and operation.

The ranking of the parameters from the Design of Experiment approach can be used to draw general guidelines in order to obtain the best fluid mechanic performance of a DBD, that are its generation of thrust and its force efficiency.

7.1. Design of a DBD.

Before designing an actuator, it is desirable to already determine a nominal operating and maximum voltage, since the input voltage strongly influences the thrust generated and the power consumed by a DBD. A higher operating voltage typically results in greater thrust generation but is often limited by the available power source in a practical implementation and dielectric materials available.

The conclusions of the present systematic study of the parameters and their interactions are that at the nominal voltage, a DBD with a thin dielectric layer of low permittivity, short inter-electrode gap, and narrow and thin air-electrode should be used in order to achieve the greatest achievable thrust. However, the dielectric thickness and permittivity must be chosen so that the electric breakdown of the material is not reached at the maximum operating voltage. Concerning the width of the encapsulated electrode, the values employed in the present study did not show an influence. However, it is known that a narrow encapsulated electrode can constrain the plasma extent and reduce the maximum achievable thrust of a DBD [13, 15, 17]. Several other parameters such as the shape of the exposed electrode and the shape of the waveform were not considered in this present work.

An additional important effect that is not discussed is the saturation of the thrust found by Thomas *et al* [15]. In the current study, the saturation was not determined to impact the results. However at higher voltages it may be important. If the operating conditions differ significantly from the present study, then the saturation frequency should be determined at the nominal and maximum operating voltages using optical measurements [15].

7.2. Operation of a DBD.

Once the design of the actuator has been chosen, the actuator can be employed in two different manners. If the goal of the application is to obtain the maximum thrust, the frequency of the input sine-wave should be increased starting from a low value. However, the frequency should always be less than the saturation frequency of the actuator at the chosen operating voltage. If the frequency exceeds the saturation frequency at a given voltage, then the thrust will be at its maximum value but with a decreased efficiency. If the DBD is used over a range of voltages and if the frequency is not modulated, the higher limit of the frequency should be less than or equal to the saturation frequency at the maximum operating voltage. In addition, the maximum deliverable power by the electric power supply should also be considered due to distortion.

On the other hand, if the force efficiency of the actuator is important for the particular application, the operating frequency can be kept at a much lower value than the saturation frequency. Nevertheless, as discussed in section 1, modulating the input signal can be beneficial for flow control applications [7, 10, 12]. Hence, it can be preferable to design a DBD and its power supply to achieve a high thrust generation and then benefit from the modulation of the signal in order to reduce the power consumption and increase the control authority of the DBD.

8. Conclusion

The purpose of the current study was to systematically rank and quantify the parameters, including the interactions between parameters, that affect the fluid mechanic performance of a DBD actuator using a Design of Experiment approach. The performance was determined by measuring the thrust generation, power consumption and force efficiency.

The thrust generation increases with voltage, and a short separation of the electrodes with a thin dielectric and short inter-electrode gap. A high AC frequency was also observed to increase the thrust. Although a high frequency was observed to increase the thrust on average, it can be detrimental for the efficiency of the DBD. The geometry of the exposed electrode was found to be significant, and a narrow and thin electrode led to an increase in the thrust generated. However, a narrow exposed electrode was observed to generate plasma on both its edges, leading to two wall jets travelling in opposite directions.

The power consumption was found to be predominantly influenced by the frequency and voltage, with an increased consumption at high frequency and/or voltage. Secondly, a short inter-electrode gap and thin dielectric layer between the electrodes led to an increase in the power consumption.

The force efficiency (the ratio of thrust to power consumed) was a useful measure to determine which of the parameters were more crucial for the thrust generation or power consumption. A higher voltage increased the efficiency, but a low frequency resulted in a greater efficiency due to the different effects of the two variables on thrust and power consumed. The separation of the electrode was the third effect, with a gain in efficiency with a short gap and thin dielectric. The geometry of the air electrode was the next parameter in the ranking, with an increase in efficiency for a thin and narrow electrode. This showed the loss of power through the dual discharges for a narrow electrode is out-weighed by the gain in thrust it creates. Finally, the interactions of the permittivity of the dielectric layer with its thickness and with the inter-electrode gap showed that the force efficiency of a DBD can be slightly increased by lowering the dielectric permittivity. In addition to the individual effects of the voltage and frequency, the interaction of the two parameters show that a combined reduction of the frequency and increase of the voltage strengthen the individual effects and leads to a greater increase in force efficiency.

The ranking of the effects that is provided by the DOE allows guidelines for the design and operation of a DBD to be determined with the caveat that with design parameters must have values similar to those employed in the present work. First, the design of a DBD should be based on an operating voltage, since this parameter drives the generation of thrust and force efficiency of a DBD. The present study concludes that a DBD that is the most effective in converting electrical power into an injection of momentum into the flow has a thin dielectric of low permittivity, a short, or no, inter electrode gap, and a narrow and thin air exposed electrode. When operating the actuator, the maximum thrust generation can be obtained by setting the frequency to a low setting and increasing it until the distortion of the power supply signal or the saturation of the thrust is encountered. If the DBD is required to have a high force efficiency, the frequency can be reduced.

9. Acknowledgements

All data supporting this study are openly available from the University of Southampton repository at `https://doi.org/10.5258/SOTON/D1415`.

References

[1] Glauert M B 1956 *Journal of Fluid Mechanics* **1** 625643 URL `https://doi.org/10.1017/S002211205600041X`

[2] Murphy J P, Kriegseis J and Lavoie P 2013 *Journal of Applied Physics* **113** 243301 (*Preprint* `https://doi.org/10.1063/1.4811225`) URL `https://doi.org/10.1063/1.4811225`

[3] Grundmann S and Tropea C 2007 *Experiments in Fluids* **42** 653–657 ISSN 1432-1114 URL `https://doi.org/10.1007/s00348-007-0256-8`

[4] Grundmann S and Tropea C 2008 *Experiments in Fluids* **44** 795–806 ISSN 1432-1114 URL `https://doi.org/10.1007/s00348-007-0436-6`

[5] Riherd M and Roy S 2014 *Journal of Physics D: Applied Physics* **47** 125203 URL `https://doi.org/10.1088%2F0022-3727%2F47%2F12%2F125203`

[6] Benard N, Braud P, Jolibois J and Moreau E 2008 *Airflow Reattachment Along a NACA 0015 Airfoil by Surfaces Dielectric Barrier Discharge Actuator: Time-Resolved Particle Image Velocimetry Investigation* (American Institute of Aeronautics and Astronautics) Fluid Dynamics and Co-located Conferences URL `https://doi.org/10.2514/6.2008-4202`

[7] Little J, Nishihara M, Adamovich I and Samimy M 2010 *Experiments in Fluids* **48** 521–537 ISSN 1432-1114 URL `https://doi.org/10.1007/s00348-009-0755-x`

[8] Moreau E 2007 *Journal of Physics D: Applied Physics* **40** 605–636 URL `https://doi.org/10.1088%2F0022-3727%2F40%2F3%2Fs01`

[9] Kriegseis J, Duchmann A, Tropea C and Grundmann S 2013 *Journal of Applied Physics* **114** 053301 URL `https://doi.org/10.1063/1.4817366`

[10] Corke T C, Enloe C L and Wilkinson S P 2010 *Annual Review of Fluid Mechanics* **42** 505–529 (*Preprint* `https://doi.org/10.1146/annurev-fluid-121108-145550`) URL `https://doi.org/10.1146/annurev-fluid-121108-145550`

[11] Liu Y, Kolbakir C, Hu H and Hu H 2018 *International Journal of Heat and Mass Transfer* **124** 319–330 ISSN 00179310 URL `https://doi.org/10.1016/j.ijheatmasstransfer.2018.03.076`

[12] Benard N, Jolibois J and Moreau E 2009 *Journal of Electrostatics* **67** 133–139 ISSN 03043886 URL https://doi.org/10.1016/j.elstat.2009.01.008

[13] Forte M, Jolibois J, Pons J, Moreau E, Touchard G and Cazalens M 2007 *Experiments in Fluids* **43** 917–928 URL https://doi.org/10.1007/s00348-007-0362-7

[14] Forte M, Jolibois J, Moreau E, Touchard G and Cazalens M 2006 *Optimization of a Dielectric Barrier Discharge Actuator by Stattionary and Non-stationary Measurements of the Induced Flow Velocity - Application to Airflow Control* (American Institute of Aeronautics and Astronautics) Fluid Dynamics and Co-located Conferences URL https://doi.org/10.2514/6.2006-2863

[15] Thomas F O, Corke T C, Iqbal M, Kozlov A and Schatzman D 2009 *AIAA Journal* **47** 2169–2178 ISSN 0001-1452 URL https://doi.org/10.2514/1.41588

[16] Hoskinson A, Hershkowitz N and Ashpis D 2009 *Comparisons of Force Measurement Methods for DBD Plasma Actuators in Quiescent Air* (American Institute of Aeronautics and Astronautics) Aerospace Sciences Meetings URL https://doi.org/10.2514/6.2009-485

[17] Enloe C L, McLaughlin T E, Van Dyken R D, Kachner K D, Jumper E J, Corke T C, Post M and Haddad O 2004 *AIAA Journal* **42** 595–604 ISSN 0001-1452 URL https://doi.org/10.2514/1.3884

[18] Debien A, Benard N and Moreau E 2012 *Journal of Physics D: Applied Physics* **45** 215201 URL https://doi.org/10.1088%2F0022-3727%2F45%2F21%2F215201

[19] Abe T, Takizawa Y, Sato S and Kimura N 2008 *AIAA Journal* **46** 2248–2256 ISSN 0001-1452 URL https://doi.org/10.2514/1.30985

[20] Corke T C, Post M L and Orlov D M 2007 *Progress in Aerospace Sciences* **43** 193 – 217 ISSN 0376-0421 URL http://www.sciencedirect.com/science/article/pii/S0376042107000486

[21] Kriegseis J, Moller B, Grundmann S and Tropea C 2011 *Journal of Electrostatics* **69** 302 – 312 ISSN 0304-3886 URL http://www.sciencedirect.com/science/article/pii/S030438861100060X

[22] Enloe C L, McLaughlin T E, Van Dyken R D, Kachner K D, Jumper E J and Corke T C 2004 *AIAA Journal* **42** 589–594 ISSN 0001-1452 URL https://doi.org/10.2514/1.2305

[23] Jolibois J and Moreau E 2009 *IEEE Transactions on Dielectrics and Electrical Insulation* **16** 758–767 ISSN 1070-9878 URL https://doi.org/10.1109/TDEI.2009.5128516

[24] Pons J, Moreau E and Touchard G 2005 *Journal of Physics D: Applied Physics* **38** 3635–3642 URL https://doi.org/10.1088%2F0022-3727%2F38%2F19%2F012

[25] Balcon N, Benard N, Lagmich Y, Boeuf J P, Touchard G and Moreau E 2009 *Journal of Electrostatics* **67** 140–145 ISSN 0304-3886 URL https://doi.org/10.1016/j.elstat.2009.01.019

[26] Abe T, Takizawa Y, Sato S and Kimura N 2007 *A Parametric Experimental Study for Momentum Transfer by Plasma Actuator* (American Institute of Aeronautics and Astronautics) Aerospace Sciences Meetings URL https://doi.org/10.2514/6.2007-187

[27] Unfer T and Boeuf J P 2010 *Plasma Physics and Controlled Fusion* **52** 124019 URL https://doi.org/10.1088%2F0741-3335%2F52%2F12%2F124019

[28] Benard N, Zouzou N, Claverie A, Sotton J and Moreau E 2012 *Journal of Applied Physics* **111** 033303 ISSN 0021-8979 URL https://doi.org/10.1063/1.3682568

[29] Anderson M J and Whitcomb J P 2015 *DOE Simplified: Practical Tools for Effective Experimentation* 3rd ed (New York: Productivity Press) ISBN 9781482218947 URL https://doi.org/10.1201/b18479

[30] Kriegseis J, Grundmann S and Tropea C 2012 *Physics of Plasmas* **19** 073509 (*Preprint* https://doi.org/10.1063/1.4736995) URL https://doi.org/10.1063/1.4736995